Suresh, L., Vaghasiya, J., Nandakumar, D. K., Wu, T., Jones, M., & Tan, S. C. (2019). High-Performance UV Enhancer Molecules Coupled with Photosynthetic Proteins for Ultra-Low-Intensity UV Detection. *Chem*, *5*(7), 1847-1860. https://doi.org/10.1016/j.chempr.2019.04.017

High performance UV enhancer molecules coupled with photosynthetic proteins for ultra-low intensity UV detection

Lakshmi Suresh,[1,3] Jayraj V. Vaghasiya,[1,3] Dilip Krishna Nandakumar,[1] Tingfeng Wu,[1] Michael R. Jones,[2] Swee Ching Tan[1,4,]*

[1]Department of Materials Science and Engineering, National University of Singapore, 9 Engineering Drive 1, Singapore 117574

[2]School of Biochemistry, Biomedical Sciences Building, University of Bristol, University Walk, Bristol BS8 1TD, UK.

[3]These authors contributed equally.

[4]Lead Contact

[*]Corresponding Author: msetansc@nus.edu.sg *(S.C. Tan)*

Summary

Dual attributes of UV-photoresponsive organic-ionic conductors are exploited in bio-photoelectrochemical cells based on photosynthetic RC-LH1 proteins from *Rhodobacter sphaeroides*. These UV-enhancer molecules (UVEM) can generate small photocurrents in the absence of protein and are also effective electrolytes for photocurrent generation by RC-LH1 complexes in response to near-infrared excitation. Mixing RC-LH1 and UVEM components strongly enhanced UV photocurrents relative to those obtained with protein or UVEM alone, an effect that is attributed to energy transfer from the heteroanthracene chromophore of the UVEM to the carotenoids of the RC-LH1 complex. RC-LH1/UVEM bio-photoelectrochemical cells were superior to conventional RC-LH1 cells in terms of UV external quantum efficiency, photo-response sensitivity and photocurrent rise-decay times. These bio-photodetectors could detect weak UV radiation with intensities as low as 2 μW/cm^2. This combination of photosynthetic proteins with dual-function electrolytes is the first attempt to construct fully-functional bio-photoelectrochemical UV photodetector based on natural components.

Keywords: Bio-photoelectrochemical cell, FRET, organic UV enhancer molecule, UV-detector, ultra-low intensity UV detection.

Introduction

Over the past two decades the development of new ultraviolet (UV) detectors has drawn extensive attention owing to their versatility in applications with scientific, technical, environmental, medical and military relevance. [1-5] An important driver of this research is concern over how human activity is impacting on the ability of stratospheric ozone to absorb UV radiation and the complex links between climate change, ozone depletion and UV exposure.[6,7] Despite the positive role played by UV B in the biosynthesis of vitamin D in the skin, most forms of UV, especially UV A and UV B, can penetrate the hypodermis and dermis to cause cell damage.[8] Safe exposure limits restrict humans in the range of 180 nm - 400 nm to 30 J m^{-2} and, specifically, to only 3 mJ cm^{-2} s^{-1} at 270 nm.[8] One area of particular interest is the development of self-powered UV photodetectors that make use of the broader spectrum to provide the power for UV detection, employ circuitry that is less heavy and more economical, and can power associated functions such as wireless data transmission.[6]

One attractive route to a self-powering UV detector is through the adaptation of a photovoltaic device for solar energy conversion. However, well-established photovoltaic devices based on silicon are susceptible to degradation from UV light exposure. As a consequence, high energy UV cannot be harnessed for energy generation by such devices and these material limitations make it difficult to develop silicon-based photodetectors despite their good sensitivity and efficiency.[9-11] Wide band gap semiconductors such as TiO_2, GaN, ZnO and SiC have been used for the fabrication of UV detectors that display a good wavelength sensitivity and fast photo-response.[1-5,12] However, in addition to complications associated with their large size and weight, use of heavy metals like cadmium, complex assembly processes and high production costs, a major drawback of semiconductor-based photodetectors is a requirement to use amplifiers and high precision measurement systems to detect the very low photocurrents produced due to low intensity UV.[5]

An area of growing interest is the use of natural photosynthetic pigment-proteins for alternative technologies to burning of fossil fuels such as bio-photoelectrochemical cells (BPECs).[13,14] In these, the light capture, charge separation and radical pair stabilization are brought about by chlorophylls, bacteriochlorophylls, carotenoids, quinones and iron-sulphur centres incorporated in a variety of combinations into light harvesting proteins and reaction centres (RCs).[15] RCs are highly effective solar energy

conversion systems, capable of operating at close to 100 % quantum efficiency (charges separated per photon absorbed).[16,17] The simplest RC that has been assembled into a BPEC is that from the purple photosynthetic bacterium *Rhodobacter (Rba.) sphaeroides*,[17-20] and numerous studies have explored its potential for technologies based on solar energy conversion.[21-24] RCs contain four bacteriochlorophylls (BChls), comprising the primary electron donor BChl pair (P) and two monomeric BChls, B_A and B_B (**Figure 1a**). The remaining cofactors are two bacteriopheophytins (BPhe - H_A and H_B), two ubiquinones (Q_A and Q_B), a carotenoid (Crt) and a Fe^{2+} atom**.** Charge separation involves photoexcitation of P to its lowest energy singlet excited state (P*), initiating transfer of the photoexcited electron sequentially to B_A, H_A, Q_A and Q_B (arrows in **Figure 1a**). At this stage, the negative and positive charges are well separated, and the $P^+Q_B^-$ state is stable for 1-5 seconds. In nature this purple bacterial RC is always enclosed in a cylindrical light harvesting 1 complex (LH1) which uses up to 32 BChls and 32 carotenoids to capture solar energy[25-28] (**Figure 1b**). As it is more strongly absorbing than a RC, the *Rba. sphaeroides*; reaction centre-light harvesting 1 (RC-LH1) complex has also been used in a variety of BPECs.[29-33]

In addition to solar energy conversion,[21-24] various applications of RCs in BPECs and on electrodes have been explored including as biosensors,[34] components for molecular electronics,[35] electrodes for solar fuel synthesis,[36] photocapacitors[37] and photosensors.[38] BPECs based on the *Rba. sphaeroides* RC or RC-LH1 complex could also form the basis of a UV detector, because these pigment-proteins have two absorbance bands in the UV range in addition to multiple absorbance bands across the visible and near-infrared spectral regions. A band with a maximum around 390 nm in RC-LH1 complexes arises from the bacteriochlorin pigments (the so-called Soret band) whereas a band with a maximum around 280 nm arises from the amino acids of the RC-LH1 protein, principally tryptophan (Trp) and tyrosine. In *Rba*. *sphaeroides* RCs it has been shown that photo-excited Trp residues undergo a fluorescence decay with a 60 ps time constant, consistent with energy transfer to the RC bacteriochlorins.[39,40] The locations of the 38 Trp residues of the *Rba. sphaeroides* RC are shown in **Figure 1a**, and those of 80 Trp residues in the cylindrical LH1 pigment-protein that surrounds the RC are shown in **Figure 1b** (and see Experimental Procedures).

Although, in principle, a RC-LH1 BPEC could act as a UV photodetector, in practice the photocurrent response to UV excitation is relatively weak. To address this, we have replaced the quinone electrolyte widely used for RC or RC-LH1 BPECs with molecules that have a dual role as a UV light absorber and a redox mediator.[40,41] These UV enhancer molecules (UVEMs) comprise twin hetero-anthracene based phenoxazine (UVEM-1) or phenothiazine (UVEM-2) donor moieties substituted with benzimidazolium iodide (BIMI) to provide an I^-/I_3^- redox mediator (**Figure 1c**).[41] These molecules absorb principally in the UV, and in previous publications these and related molecules were explored as single component solid-state electrolyte in TiO_2 dye-sensitized solar cells.[41-43] The BIMI group facilitates Grotthuss type electron transfer through a polyiodide chain and is responsible for high ionic conductivity. The role of the phenoxazine/phenothiazine donor group is to absorb light and enhance dye sensitization. In principle these UVEMs can support a photocurrent alone in a photoelectrochemical cell, the UV-absorbing moiety donating a photoexcited electron to the BIMI group to separate charge. However, interestingly, the UV absorbance and emission bands of these UVEMs overlap with absorbance bands of the RC-LH1 complex, raising the prospect that they could enhance UV photocurrent generation by acting as an auxiliary UV light harvesting system in addition to providing a redox electrolyte.

In this work we examine solar energy conversion in RC-LH1/UVEM BPECs with a focus on the response and sensitivity to UV radiation. We find that UVEMs can substitute for water-soluble quinones as an effective redox electrolyte, and simultaneously enhance the UV excitation photoresponse to an extent that implicates energy donation to the RC-LH1 complexes. Potential use of these materials in sensitive UV photodetectors is demonstrated and discussed.

Results

The assembled BPEC comprised a transparent FTO-glass front electrode, a concentrated mixture of 28.6 mM RC-LH1 complexes and 85.7 mM UVEM-1 or UVEM-2, and a Pt-coated carbon cloth back electrode (**Figure 2a**). Cells were also constructed in which the UVEM electrolyte was replaced by 85.7 mM ubiquinone-0 (Q_0), which is the conventional choice of electrolyte for cells based on purple bacterial photoproteins,[44] and control cells with just UVEM electrolyte were also constructed.

The envisaged mechanism operating in the RC-LH1/UVEM cells, consistent with known vacuum potentials and the direction of current flow, is shown in **Figure 2b**. Light absorption by the BChls and carotenoids of the RC-LH1 complex culminates in excitation of the RC primary electron donor BChl pair (P*) followed by charge separation to the Q_B ubiquinone of the RC to form the radical pair $P^+Q_B^-$ (**Figure 1a**), and transfer of electrons to the counter electrode by the I^-/I_3^- redox couple of the UVEMs (**Figure 2b**). The circuit is completed by hole migration to the FTO-glass front electrode, either by direct transfer (as shown) or mediated by the electrolyte (**Figure 2b**). From the point of view of electron transfer, this mechanism is similar to that proposed previously for RC-LH1 photoelectrochemical cells employing Q_0 or a variety of alternative mediators.[29-34,44] The novel aspect of this new cell design was the use of the photo-responsive UVEM electrolyte which brings the possibility of enhanced current flow through two mechanisms (**Figure 2b**). The first is oxidation (reduction) of the photo-excited UVEM electrolyte at the anode(cathode) with no involvement of the RC-LH1 protein. The second involves both nonradiative and radiation assisted energy transfer between the UV-absorbing phenoxazine or phenothiazine moiety of the UVEM and the visible-absorbing multi-chromophore RC-LH1 complex, with current flow then driven by normal RC-LH1 photochemistry.

The UVEM-1 and UVEM-2 electrolytes exhibited absorbance maxima at 376 nm and 352 nm respectively, with a second band at ~270 nm (**Figure 2c**, black). The first of these bands either completely or partially coincided with the Soret absorbance band of the RC-LH1 bacteriochlorophylls at 372 nm, and the second overlapped the RC-LH1 protein absorbance band at 280 nm (**Figure 2c**, red). The effect of mixing either UVEM-1 or UVEM-2 with the RC-LH1 complex was therefore to enhance absorbance in the UV A (315-400 nm) regions and at the interface between the UV B (280-315 nm) and UV C (100-280 nm) regions. UV excitation of either UVEM produced visible region emission (see insets to **Figure 2c**), the emission bands of UVEM-1 and UVEM-2 (**Figure 2c**, green) overlapping with the broad RC-LH1 absorbance band between 450 nm and 600 nm that arises largely from the spheroidenone carotenoids of the LH1 protein (32 per RC-LH1 complex). Adding either UVEM to the RC-LH1 complex resulted in over 90 % absorbance of UV light at 365 nm and 50 % absorbance at 254 nm (**Figure 2d**).

The roles of different cell components were examined by recording external quantum efficiency (EQE) action spectra. Cells without RC-LH1 complexes

(FTO/UVEM/carbon cloth) gave a low EQE response with a line shape that approximated to the absorbance spectrum of each UVEM between 300 and 700 nm, with maximal efficiencies at 370 nm (UVEM-1) and 363 nm (UVEM-2) (inset to **Figure 2e)**). This showed that these photo-responsive electrolytes were able to generate a photocurrent in the absence of the RC-LH1 protein. Cells fabricated from a mixture of RC-LH1 and Q_0 yielded a multi-band EQE spectrum with bands above 700 nm and centered at 386 nm attributable to the LH1 and RC BChls, and a broad band between 450 and 650 nm attributable mainly to the LH1 carotenoids (**Figure 2e**). The maximum EQE in the UV, at around 0.048 %, was 5 to 10-fold higher than that obtained with UVEM-1 or UVEM-2 alone (**Figure 2e**). Mixing UVEM-1 or UVEM-2 with the RC-LH1 complex did not increase the EQE in the region above 650 nm. However, the photocurrent response across the visible and, in particular, UV region was enhanced, with a maximum of 0.086 % at 381 nm for UVEM-1 and 0.066% at 378 nm for UVEM-2. This enhancement was 4-5-fold larger than could be accounted for by direct photocurrent generation by either UVEM-1 or UVEM-2 alone, and we attribute it to energy transfer from the UVEM chromophores to the carotenoids of the RC-LH1 complex. The spectral overlap illustrated in **Figure 2c** would be consistent with Förster resonance energy transfer (FRET) from the phenoxazine or phenothiazine moiety of the UVEM to the 32 carotenoid cofactors of each RC-LH1 complex, and/or carotenoid absorption of UVEM emission.

Evidence for energy transfer was obtained by measuring excited state lifetimes of the UVEM molecules with and without RC-LH1 complexes by time-resolved photoluminescence. Accurate fitting of decay curves required a tri-exponential function (**Figure S1**); lifetime parameters are collated in Supplemental Information, **Table S1**. Average lifetimes for emission decay ($\langle\tau\rangle$) in the absence of RC-LH1 were 1728 ps for UVEM-1 and 1415 ps for UVEM-2. When RC-LH1 were mixed with either UVEM there was a drastic decrease in the average lifetime to 335 ps for UVEM-1/RC-LH1 and 539 ps for UVEM-2/RC-LH1. This validated an energy transfer mechanism between the UVEM donor and RC-LH1 acceptor. The percentage energy transfer efficiency (η_{FRET}, %) was calculated for both mixtures from the ratio of amplitude-weighted lifetimes (τ_{amp} - see **Table S1**). Energy transfer from UVEM-1 to RC-LH1 exhibited an efficiency of 74.1% and UVEM-2 to RC-LH1 exhibited a slightly lower efficiency of 61.6%.

Responses of the BPECs to UV excitation were also measured by photo-chronoamperometry with illumination at 365 nm or 254 nm (average photocurrents are compiled in **Table 1**). UVEM-only cells generated photocurrents of the order of a few tens of nA cm^{-2} (**Figure 3a**), with ~3-fold higher currents seen with 365 nm excitation (intensity 1350 μW cm^{-2}, **Figure 3a, left**) than 254 nm excitation (intensity 110 μW cm^{-2}, **Figure 3a, right**). A consistently somewhat higher output was obtained from UVEM-1 cells than UVEM-2 cells under either type of excitation (**Figure 3a**), in accord with their relative responses in EQE action spectra (**Figure 2e**, inset). Average photocurrents from RC-LH1 cells with UVEM-1 or UVEM-2 as electrolyte were higher than those with Q_0 as electrolyte (**Figure 3b, c**), with the highest output being obtained with UVEM-1; again, photocurrents were higher with 365 nm excitation than with 254 nm excitation in all cases. Photocurrents produced by RC-LH1/UVEM cells showed an initial decline that stabilised after ~15 s; this effect was likely due to limitations produced by mediator diffusion as discussed previously.[33]

The relative outputs of the RC-LH1/UVEM cells were stable over time, as assessed from light-on/light-off measurements repeated at 100 sec intervals (**Figure 3d**). Further, the stability of RC-LH1/UVEM-1 cells under 5-hour periods of outdoor sunlight or UV irradiation (1350 μW cm^{-2}, 365nm) was monitored over a period of 10 days (Supplemental Information, **Figure S2)**. Cell contents (**Figure S2a, b**) and output (**Figure S2c**) showed good stability in either case, with a decrease in output of only ~10 % over this period.

Photocurrent rise times (τ_{rise}) and decay times (τ_{decay}) in response to UV excitation of RC-LH1 cells are compared in **Figure 4a, b** (values in supplemental information **Table S2**. The detector recorded a τ_{rise} of ~0.54 s and ~0.70 s under 365 nm illumination and ~0.44 s and ~0.60 s under 254 nm illumination for UVEM-1 and UVEM-2, respectively, with very good reproducibility under repeated cycles of light-on/light-off. In contrast the response of the RC-LH1/Q_0 cells was much slower, with a τ_{rise} and τ_{decay} of a few seconds with either type of illumination (**Figure 4a, b**). These results indicated that the RC-LH1 cells with an UVEMs were quicker in detecting UV radiation than cells with Q_0, possibly because their output is less dependent on mediator diffusion through the device.

Another key characteristic for validating a bio-photodetector is its sensitivity. As shown in **Figure 4c, d**, for both 365 nm and 254 nm excitation the photocurrent amplitude scaled with light intensity. At the lowest intensity tested, 2 μW cm^{-2},

measurable photo-responses were obtained with either UVEM and with either wavelength of excitation. However, RC-LH1/Q_0 tested under similar conditions under varying intensities showed lower photo-responses thus confirming that UVEMs boost the UV detectability of RC-LH1.

The photovoltage response of the RC-LH1/UVEM-1 BPEC was maximally 310 mV under 365 nm excitation and 200 mV under 254 nm excitation (intensities of 1350 μW cm^{-2} and 110 μW cm^{-2}, respectively). The response to 365 nm excitation was intensity dependent, declining to 100 mV at 2 μW cm^{-2}. This variable photovoltage response was used as the basis of a prototype working Bio-UV sensor capable of detecting a range of UV intensities, fabricated by connecting a RC-LH1/UVEM-1 BPEC to a microcontroller board and an LED display (**Figure 5a**). The setup was programmed to display colour-coded alert symbols ("H"- high intensity, "M"- medium intensity and "L" - low intensity) when exposed to different intensities of 365 nm illumination (ranges 1350-800 μW cm^{-2}, 800-100 μW cm^{-2} and 100 to 2 μW cm^{-2}, respectively). Sensor responses illustrated in **Figure 5a** are demonstrated in **Movie S1** of Supplemental information.

As a proof of concept of a wearable detector, a demonstration RC-LH1/UVEM-1 device was constructed by replacing the glass used as substrate for the transparent front electrode with flexible polyethylene terephthalate (PET) substrate. The Pt-coated carbon cloth back electrode was retained, producing a flexible cell with a PET-ITO/RC-LH1/UVEM-1)/carbon cloth architecture. This could power a small display when exposed to a UV intensity above 200 μW cm^{-2} (**Figure 5b**).

Discussion

The typical approach to fabrication of a BPEC is to combine a photoactive RC protein with one or more redox electrodes, with the RCs either free in solution or adhered to one of the electrodes. The wavelength-dependence of the cell's photoresponse is then determined by the absorbance properties of the photoprotein, which in turn are determined by the profile of bound pigments and their connectivity (i.e. the efficiency of inter-pigment energy transfer). In addition, photosynthetic proteins contain aromatic amino acids that contribute to an absorbance band with a maximum around 280 nm, that straddles the UV-B and UV-C spectral regions. The location of the 38 Trp residues in the *Rba*. *sphaeroides* RC are shown in **Figure 1a**

and it has been estimated that around 20 of these Trp residues participate in energy transfer to its six bacteriochlorin cofactors, with a mean Trp-bacteriochlorin distance of around 20 Å.[39] Thus, provided they are sufficiently close, Trp residues can act as a UV-responsive antenna to drive RC photochemistry, and hence a BPEC photocurrent and photovoltage. The RC-LH1 complex used in the present work has an additional 80 Trp residues in the surrounding LH1 antenna (**Figure 1b**), and it is evident from the small photocurrents derived from 254 nm excitation of the RC-LH1/Q_0 cells (**Figure 3c**) that excitation of these can drive some RC photochemistry, corroborating and extending previous findings from spectroscopy.[39]

A possible way to enhance the spectral response of the protein in a BPEC is to physically attach dyes sufficiently close to the protein surface to enable energy transfer through mechanisms such FRET. Such modified RCs have been engineered and shown to engage in enhanced energy capture,[45-50] but have not been tested in a BPEC. In the present work we have established the feasibility of an alternative approach in which the small molecule electrolyte fulfils a dual function as a redox mediator and an energy harvester. For the former, consideration of the EQE spectra above 700 nm (i.e. outside the absorbance range of either UVEMs) shows that these UVEMs can replace Q_0 as effective redox mediators. To do so the UVEMs must be able to engage in a close-range physical interaction with the RC-LH1 complex (<2 nm) so that it can transfer electrons created by charge separation within the RC. In addition, the enhanced EQE seen below 600 nm, and particularly below 450 nm, demonstrates that the UVEMs are also able to transfer energy to the RC-LH1 pigments. As far as we aware this is the first example where a dual-function energy harvesting electrolyte has been used in a BPEC, and also the first example of augmentation of RC-LH1 energy harvesting by a molecule that is not physically attached through a specific binding interaction. One possibility is that the mechanism of energy transfer is FRET, with the 32 LH1 carotenoids that absorb between 400 and 600 nm acting as the energy acceptors. FRET would require an intimate interaction between RC-LH1 complexes and UVEMs that brings the participating chromophores within FRET distance, expected to be a few nm, and the effectiveness of the UVEMs as redox mediators, which requires shorter range electron transfer between the RC-LH1 quinones and the UVEMs, shows that these molecules are indeed capable of closely interacting and therefore satisfying this condition for FRET. The alternative possibility, given that both components are present at tens of millimolar concentration in the BPEC, is that energy

transfer is mediated by RC-LH1 absorption of UVEMs emission (i.e. the inner filter effect encountered in fluorescence spectroscopy of concentrated samples). These radiation-less and radiation-dependent mechanisms are not mutually exclusive and could be operating side-by-side in these UV-enhanced BPECs.

The strongest enhancement of photocurrent generation by the UVEMs was seen in the UV, as evident from the EQE spectra below 425 nm (**Figure 2e**) and from photocurrent measurements using standard UV sources with outputs peaking at 365 nm or 254 nm. These UV responses were more rapid than those obtained with Q_0 as mediator **(Figure 4a, b)**, and were obtainable at excitation intensities down to 2 μW cm^{-2}. This sensitivity is comparable to that reported for a variety of materials that have been put forward as self-powered UV photodetectors.[51,52] Thus, in addition to their potential as a UV-enhanced solar energy convertor, these BPECs could also form the basis of a UV-photodetector based on a natural photosynthetic protein and a novel, optically-active electrolyte. The demonstration summarised and shown in **Movie S1** represents the first step in this direction, using UV light to activate a warning display.

To conclude, in a recent report we demonstrated single and multi-pixel BPEC cells formed from flexible electrode materials and a gel phase electrolyte/RC-LH1 blend that were capable of touch sensing and touch tracking through pressure modulation of their open circuit voltage.[53] The electrolyte comprised the conventional mediator Q_0 dispersed throughout a plastic crystalline succinonitrile matrix, mixed in a 1:5 ratio (by volume) with the RC-LH1 protein. This prototype, self-powered “e-skin” material was UV-responsive due to the protein and BChl absorbance bands of the RC-LH1 complex, but at a ~5-fold lower sensitivity than the RC-LH1/UVEM system used in the present study. In future work it may be possible to incorporate UVEMs into this type of flexible BPEC material to enhance the sensitivity of its UV detection and also, based on the present work, the rate of signal response to harmful radiation. More generally it will also be interesting to explore, in BPECs with diverse designs and compositions, the benefits of replacing single function electrolytes with variations on the UVEM theme that have the dual function of redox mediation and the enhancement of the solar energy harvesting capacity of the cell.

Experimental procedures

Ubiquinone-0 (Q_0 - 2-3-dimethoxy-5-methyl-p-benzoquinone, 98 %) was obtained from Merck. The synthesis of UVEM-1 and UVEM-2 was performed as previously reported.[40] The PufX-deficient *Rba. sphaeroides* RC-LH1 protein was purified as described previously[33] and stored as a concentrated solution in 20 mM Tris (pH 8.0)/0.04% (w/v) n-dodecyl β-D-maltopyranoside at -80°C until use.

The device structure constituted pieces of FTO conducting glass and platinum-coated carbon cloth (ACME Research support Pte. Ltd. Singapore) separated with a paraffin spacer. This created a cavity which was filled with a mixture of 4 µL of RC-LH1 protein solution (50 mM) and 3 µL of UVEM-1 or UVEM-2 (both 0.2 M) in 0.1 M Tris-HCl (pH 8). The cells were then sealed with epoxy resin. Counterpart RC-LH1/Q_0 cells were also prepared using 3 µL of 0.2 M Q_0 in 0.1 M Tris-HCl (pH 8) instead of the UVEM solution. Protein-free cells were prepared using 10 µL of 0.2 M UVEM-1 or UVEM-2 in 0.1 M Tris-HCl (pH 8). For flexible cells, the FTO-glass front electrode was replaced by polyethylene terephthalate coated with indium tin oxide (PET-ITO - Latech Scientific Supply, Singapore).

Photo-chronoamperometry was carried out using a Keithley 2400 Source Meter under UV light irradiation from a WFH-204B Portable Ultraviolet Analyzer Lamp (5W) either at 365 nm or 254 nm. The active area of all cells was maintained at 0.2 cm^2 using a black mask with an aperture placed on the front electrode (FTO glass) before measurement. Intensity was modulated by varying the distance of the light source from the cell and was calibrated using reference standard cells and a photo-detection meter (Newport, Oriel Instruments, USA).

EQE measurements were carried out using light from a 250 W quartz tungsten halogen lamp dispersed through a monochromator and focused on the cell with a spot size smaller than the device active area. Action spectra of EQE versus excitation wavelength were calculated from the photocurrent action spectra. The incident light intensity was monitored and calibrated using a silicon photodiode. UV-visible absorption and emission spectra were measured using a UV160A spectrophotometer (Shimadzu, Japan) and Cary Eclipse Fluorescence Spectrophotometer (Agilent Technologies).

To examine photostability, RC-LH1/UVEM-1 cells were either exposed to outdoor sunlight or to high intensity (1350 µW cm^{-2}) UV light for 5 hours per day for 10 days. UV-vis absorbance spectroscopy was carried out daily to monitor the structural

(and hence functional) stability of cell contents and photo-chronoamperometry was used to monitor cell output.

For a practical demonstration (see **Movie S1** and **Scheme S1**) a simple UV detector circuit was designed using an Arduino Uno microcontroller board and a half-sized solderless breadboard. The detector BPEC was constructed as described above. The OLED display panel and BPEC were connected to the Arduino board using jumper wires. The thresholds to display “H”, “M” and “L” were set to 0.3 V, 0.2 V and 0.1 V in the code which were uploaded using Arduino IDE 1.8.5 open source software. Excitation was supplied using a WFH-204B Portable Ultraviolet Analyzer Lamp (5W) and intensity was modulated by varying the distance between lamp and BPEC.

Representations of protein structure were produced using the PyMOL Molecular Graphics System (Schrödinger, LLC). Images of the cofactor structure of the *Rba. sphaeroides* RC were produced using Protein Data Bank entry 3ZUW.[50] Colour coding for carbon atoms: yellow – P BChl pair; green – B_A/B_B BChls; pink – H_A/H_B BChls; cyan – Q_A/Q_B ubiquinones; dark-teal – carotenoid; orange – tryptophans. Oxygens were in red and nitrogens in blue. Iron was shown as an orange sphere and magnesium as a magenta sphere. Cofactor side chains and backbone atoms were not shown for clarity. Images of the cofactor structure of the RC-LH1 complex were produced using Protein Data Bank entry 3WMM for the *Thermochromatium tepidum* RC-LH1 complex.[27] This was used as it has a closed LH1 ring around the central RC, as in the PufX-deficient *Rba. sphaeroides* RC-LH1 used in the present work, and a high-resolution structure has not been determined for the latter. Colour coding for carbon atoms: yellow – RC P BChl pair; teal – LH1 BChls; dark green – LH1 carotenoid; orange – tryptophans. Oxygens in red, nitrogens in blue and magnesium as magenta sphere. BChl side chains and backbone atoms are not shown for clarity. For the UVEMs, colour coding: grey – carbon; white – hydrogen; blue – nitrogen; red – oxygen, gold – sulphur, and magenta – iodine.

Acknowledgments

Lakshmi Suresh, Jayraj V. Vaghasiya, Dilip Krishna Nandakumar and Swee Ching Tan acknowledge the financial support from MOE AcRF 1 (R-284-000-161-114). Michael R. Jones acknowledges support from the Biotechnology and Biological Sciences Research Council of thae UK (project BB/I022570/1) and the BrisSynBio

Synthetic Biology Research Centre (BB/L01386X/1). We thank Dr. Kamol Wasapinyokul for his technical discussions and support.

Author Contributions

Conceptualization, S.C.T., J.V.V. and L.S.; Experiments, J.V.V., L.S. and D.K.N.; Biological materials, M.R.J.; writing-review and editing, J.V.V., L.S., M.R.J. and S.C.T.; Synthesis, L.S. and J.V.V.; TRPL measurement, J.V.V.; Arduino setup: T.W.; Supervision, S.C.T.; J.V.V. and L.S. have contributed equally to this work.

Declaration of Interests

The authors declare no competing interests.

References and notes

1. Sang, L., Liao, M., Sumiya, M. (2013). A comprehensive review of semiconductor ultraviolet photodetectors: from thin film to one-dimensional nanostructures. Sensors 13, 10482-10518.
2. Hou, Y., Mei, Z., Du, X. (2014). Semiconductor ultraviolet photodetectors based on ZnO and $Mg_xZn_{1-x}O$. J. Phys. D: Appl. Phys. 47**,** 283001.
3. Zhou, J., Chen, L., Wang, Y., He, Y., Pan, X., Xie, E. (2016). An overview on emerging photoelectrochemical self-powered ultraviolet photodetectors. Nanoscale 8**,** 50-73.
4. Han, S. T., Peng, H., Sun, Q., Venkatesh, S., Chung, K. S., Lau, S. C., Zhou, Y., Roy, V. A. L. (2017). An overview of the development of flexible sensors. Adv. Mater. 29, 1700375.
5. Tian, W., Wang, Y., Chen, L., Li, L. Self-powered nanoscale photodetectors. (2017). Small 13, 1701848.
6. Wang, Z. L. (2012). Self-powered nanosensors and nanosystems, Adv. Mater. 24, 280-285.
7. Williamson, C. E., Zepp, R. G., Lucas, R. M., Madronich, S., Austin, A. T., Ballare, C. L., Norval, M., Sulzberger, B., Bais, A. F., McKenzie, R. L., Robinson, S. A., Hader, D. P., Paul, N. D., Bornman, J. F. (2014). Solar ultraviolet radiation in a changing climate. Nature Climate Change 4, 434-441.
8. International Commission on Non-Ionizing Radiation Protection, ICNIRP guidelines on limits of exposure to ultraviolet radiation of wavelengths between 180 nm and 400 nm (incoherent optical radiation). (2004). Health Physics 87, 171-186.
9. Rogalski, A., Razeghi, M. (1996). Semiconductor ultraviolet photodetectors, Opto-Electr. Rev. 4, 13-30.
10. Wan, X., Xu, Y., Guo, H., Shehzad, K., Ali, A., Liu, Y., Yang, J., Dai, D., Lin, C. T., Liu, L., Cheng, H. C., Wang, F., Wang, X., Lu, H., Hu, W., Pi, X., Dan, Y., Luo, J., Hasan, T., Duan, X., Li, X., Xu, J., Yang, D., Ren, T., Yu, B. (2017). A self-powered high-performance graphene/silicon ultraviolet photodetector with ultra-shallow junction: breaking the limit of silicon?. npj 2D Materials and Applications 4, 1-8.

11. Shi, L., Nihtianov, S., Nanver, L. K., Scholze, F. (2013). Stability Characterization of High-Sensitivity Silicon-Based EUV Photodiodes in a Detrimental Environment, IEEE Sensor Journal 13, 1699-1707.
12. Morkoc, H., Strite, S., Gao, G. B., Lin, M. E., Sverdlov, B., Burns, M. J. (1994). Large band-gap SiC, III-V nitride, and II-VI ZnSe-based semiconductor device technologies. Appl. Phys. 76, 1363.
13. Nandakumar, D.K., Ravi, S.K., Zhang, Y., Guo, N., Zhang, C., and Tan, S.C. (2018). A super hygroscopic hydrogel for harnessing ambient humidity for energy conservation and harvesting. Energy & Environmental Science 11, 2179-2187.
14. Singh, V.K., Ravi, S.K., Ho, J.W., Wong, J.K.C., Jones, M.R., and Tan, S.C. (2018). Biohybrid Photoprotein-Semiconductor Cells with Deep-Lying Redox Shuttles Achieve a 0.7 V Photovoltage. Advanced Functional Materials 28, 1703689.
15. Heathcote, P., Jones, M. R. (2012). The structure-function relationships of photosynthetic reaction centres. Comprehensive Biophysics, ed E.H. Egelman, and S. Ferguson, 8, 115-144. Academic Press, Oxford, UK.
16. Scholes, G. D., Fleming, G. R., Olaya-Castro, A., van Grondelle, R. (2011). Lessons from nature about solar light harvesting. Nat. Chem. 3, 763-774.
17. Jones, M. R. (2009). The petite purple photosynthetic powerpack. Biochem. Soc. Trans. 37, 400-407.
18. Feher, G., Allen, J. P., Okamura, M. Y., Rees, D. C. (1989). Structure and function of bacterial photosynthetic reaction centres. Nature 339, 111-116.
19. Allen, J., Williams, J. (1998). Photosynthetic reaction centers. FEBS Letters 438, 5-9.
20. Zinth, W., Wachtveitl, J. (2005). The first picoseconds in bacterial photosynthesis - ultrafast electron transfer for the efficient conversion of light energy. ChemPhysChem 6, 871-880.
21. Kim, Y., Shin, S. A., Lee, J., Yang, K. D., Nam, K. T. (2014). Hybrid system of semiconductor and photosynthetic protein. Nanotechnology 25, 342001.

22. Yehezkeli, O., Tel-Vered, R., Michaeli, D., Willner, I., Nechushtai, R. (2014). Photosynthetic reaction center-functionalized electrodes for photo-bioelectrochemical cells. Photosynth. Res. 120, 71-85
23. Ravi, S. K., Tan, S. C. (2015). Progress and perspectives in exploiting photosynthetic biomolecules for solar energy harnessing. Energy Environ. Sci. 8, 2551-2573.
24. Ravi, S. K., Udayagiri, V. S., Suresh, L., Tan, S. C. (2017). Emerging Role of the Band-Structure Approach in Biohybrid Photovoltaics: A Path Beyond Bioelectrochemistry. Adv. Funct. Mater. 28, 1705305.
25. Qian, P., Papiz, M. Z., Jackson, P. J., Brindley, A. A., Ng, I. W., Olsen, J. D., Dickman, M. J., Bullough, P. A., Hunter, C. N. (2013). Three-dimensional structure of the *Rhodobacter sphaeroides* RC-LH1-PufX complex: Dimerization and quinone channels promoted by PufX. Biochemistry 52, 7575-7585.
26. Qian, P., Siebert, C. A., Wang, P., Canniffe, D. P., Hunter, C. N. (2018). Cryo-EM structure of the *Blastochloris viridis* LH1–RC complex at 2.9 Å. Nature 556**,** 203-208.
27. Niwa, S., Yu, L. J., Takeda, K., Hirano, Y., Kawakami, T., Wang-Otomo, Z. Y., Miki, K. (2014). Structure of the LH1-RC complex from Thermochromatium tepidum at 3.0 angstrom. Nature 508, 228-232.
28. Yu, L. J., Suga, M., Wang-Otomo Z. Y., Shen, J. R. (2018). Structure of photosynthetic LH1-RC supercomplex at 1.9 angstrom resolution, Nature 556, 209-213.
29. Tan, S.C., Crouch, L. I., Mahajan, S., Jones, M. R., Welland, M. E. (2012). Increasing the open circuit voltage of photoprotein-based photoelectrochemical cells by manipulation of the vacuum potential of the electrolytes. ACS Nano 6, 9103-9109.
30. Tan, S. C., Yan, F., Crouch, L. I., Robertson, J., Jones M. R., Welland, M. E. (2013). Superhydrophobic Carbon Nanotube Electrode Produces a Near-Symmetrical Alternating Current from Photosynthetic Protein-Based Photoelectrochemical Cells. Adv. Funct. Mater. 23, 5556-5563.
31. Yaghoubi, H., Lafalce, E., Jun, D., Jiang, X. M, Beatty, J. T., Takshi, A. (2015). Large photocurrent response and external quantum efficiency in

biophotoelectrochemical cells incorporating reaction center plus light harvesting complexes. Biomacromolecules, 16, 1112-1118.

32. Ravi, S. K., Swainsbury, D. J. K., Singh, V. K., Ngeow, Y. K., Jones, M. R., Tan, S. C. (2018). A Mechanoresponsive Phase-Changing Electrolyte Enables Fabrication of High-Output Solid-State Photobioelectrochemical Devices from Pigment-Protein Multilayers. Adv.Mater. 30, 1704073.
33. Friebe, V. M., Delgado, J. D., Swainsbury, D., Gruber, J. M., Chanaewa, A., van Grondelle, R., von Hauff, E., Millo, D. Jones, M., Frese, R. N. (2016). Plasmon-Enhanced Photocurrent of Photosynthetic Pigment Proteins on Nanoporous Silver. Adv. Funct. Mater. 26, 285-292.
34. Swainsbury, D. J., Friebe, V. M., Frese, R. N., Jones, M. R. (2014). Evaluation of a Biohybrid Photoelectrochemical Cell Employing the Purple Bacterial Reaction Centre as a Biosensor for Herbicides. Biosens. Bioelectron. 58 , 172–178.
35. Wang, F., Liu, X., Willner, I. (2013). Integration of photoswitchable proteins, photosynthetic reaction centers and semiconductor/biomolecule hybrids with electrode supports for optobioelectronic applications. Adv. Mater. 25, 349-377.
36. Efrati, A., Lu, C. H., Michaeli, D., Nechushtai, R., Alsaoub, S., Schuhmann, W., Willner, I. (2016). Assembly of Photo-Bioelectrochemical Cells Using Photosystem I-Functionalized Electrodes. Nat. Energy 1, 15021.
37. Ravi, S.K., Rawding, P., Elshahawy, A.M., Huang, K., Sun, W., Zhao, F., Wang, J., Jones, M.R. and Tan, S.C. (2019) Photosynthetic apparatus of Rhodobacter sphaeroides exhibits prolonged charge storage. Nature Communications 10, 902.
38. Terasaki, N., Yamamoto, N., Tamada, K., Hattori, M., Hiraga, T., Tohri, A., Sato, I., Iwai, M., Iwai, M., Taguchi, S., Enami, I., Inoue, Y., Yamanoi, Y., Yonezawa, T., Mizuno, K., Murata, M., Nishihara, H., Yoneyama, S., Minakata, M., Ohmori, T., Sakai. M., Fujii, M. (2007). Bio-Photosensor: Cyanobacterial Photosystem I Coupled with Transistor via Molecular Wire. Biochim. Biophys. Acta - Bioenerg. 1767,653-659.
39. Godik, V. I., Blankenship, R. E., Causgrove T. P., Woodbury, N. (1993). Time-resolved tryptophan fluorescence in photosynthetic reaction centers from *Rhodobacter sphaeroides*. FEBS Letters, 321, 229-232.

40. Ravi, S.K., Yu, Z., Swainsbury, D.J.K., Ouyang, J., Jones, M.R., and Tan, S.C. (2017). Enhanced Output from Biohybrid Photoelectrochemical Transparent Tandem Cells Integrating Photosynthetic Proteins Genetically Modified for Expanded Solar Energy Harvesting. Advanced Energy Materials 7, 1601821.
41. Vaghasiya, J. V., Sonigara, K. K., Soni, S. S., Tan, S. C. (2018). Dual functional hetero-anthracene based single component organic ionic conductors as redox mediator cum light harvester for solid state photoelectrochemical cells. J. Mater. Chem. A, 6, 4868-4877.
42. Vaghasiya, J.V., Sonigara, K.K., Suresh, L., Panahandeh-Fard, M., Soni, S.S., and Tan, S.C. (2019). Efficient power generating devices utilizing low intensity indoor lights via non-radiative energy transfer mechanism from organic ionic redox couples. Nano Energy 60, 457-466.
43. Vaghasiya, J. V., Sonigara, K. K., Prasad, J., Beuvier, T., Gibaud, A., Soni, S. S. (2017). Role of a phenothiazine/phenoxazine donor in solid ionic conductors for efficient solid state dye sensitized solar cells. J. Mater. Chem. A, 5, 5373-5382.
44. Friebe, V. M., Swainsbury, D. J. K., Fyfe, P. K., van der Heijden, W., Jones, M. R., Frese, R. N. (2016). On the mechanism of ubiquinone mediated photocurrent generation by a reaction center based photocathode. Biochimica et Biophysica Acta Bioenergetics 1857, 1925-1934.
45. Milano, F. , Tangorra, R. R., Hassan Omar, O., Ragni, R., Operamolla, A., Agostiano, A., Farinola, G. M., Trotta, M. (2012). Enhancing the Light Harvesting Capability of a Photosynthetic Reaction Center by a Tailored Molecular Fluorophore. Angew. Chemie - Int. Ed. 51,11019-11023.
46. Dutta, P. K., Lin, S., Loskutov, A., Levenberg, S., Jun, D., Saer, R. , Beatty, J. T., Liu, Y., Yan, H. and Woodbury, N. W. (2014). Reengineering the Optical Absorption Cross-Section of Photosynthetic Reaction Centers. J. Am. Chem. Soc. 136,4599-4604.
47. Dutta, P. K., S. Levenberg, Loskutov, A., Jun, D., Saer, R., Beatty, J. T., Lin, S., Liu, Y., Woodbury, N. W., Yan, H. (2014). A DNA-Directed Light-Harvesting/reaction Center System. J. Am. Chem. Soc. 136, 16618-16625.
48. Operamolla, A., Ragni, R., Milano, F., Roberto T. R., Antonucci, A., Agostiano, A., Trotta, M., Farinola, G. (2015). “Garnishing” the Photosynthetic Bacterial

Reaction Center for Bioelectronics. J. Mater. Chem. C 3, 6471-6478.

49. Hassan O. O., La Gatta, S., Tangorra, R. R., Milano, F., Ragni, R., Operamolla, A., Argazzi, R., Chiorboli, C., Agostiano, A., Trotta, M., Farinola, G. M. (2016). Synthetic Antenna Functioning As Light Harvester in the Whole Visible Region for Enhanced Hybrid Photosynthetic Reaction Centers. Bioconjug. Chem. 27, 1614-1623.
50. Grayson, K. J., Faries, K. M., Huang, X., Qian, P., Dilbeck, P., Martin, E. C., Hitchcock, A., Vasilev, C., Yuen, J. M., Niedzwiedzki, D. M., Leggett, G. J., Holten, D., Kirmaier, C., Hunter, C. N. (2017). Augmenting Light Coverage for Photosynthesis through YFP-Enhanced Charge Separation at the *Rhodobacter sphaeroides* Reaction Centre. Nat. Commun. 8, 1-12.
51. Gao, C., Li, X., Wang, Y., Chen, L., Pan, X., Zhang, Z., Xie, E. (2013). Titanium dioxide coated zinc oxide nanostrawberry aggregates for dye-sensitized solar cell and self-powered UV-photodetector. J. Power Sources 239, 458-465.
52. Li, X., Gao, C., Duan, H., Lu, B., Pan, X., Xie, E. (2012). Nanocrystalline TiO_2 film based photoelectrochemical cell as self-powered UV-photodetector. Nano Energy 1, 640-645.
53. Ravi, S. K., Wu, T. Udayagiri, V. S., Vu, X. M., Wang, Y., Jones, M. R., Tan, S. C. (2018). Photosynthetic Bioelectronic Sensors for Touch Perception, UV-Detection, and Nanopower Generation: Toward Self-Powered E-Skins. Adv. Mater. 30, 1802290.

Figure and Table legends

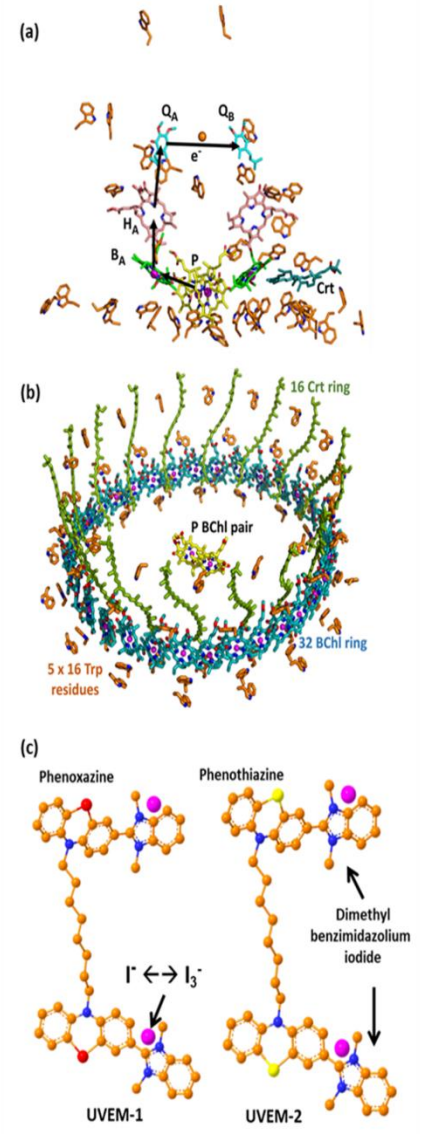

Figure 1. Structures of components. (a) Arrangement of 38 UV-absorbing Trp residues in the vicinity of the RC cofactors that carry out charge separation (black arrows). (b) The RC (represented by the P BChl pair only) is surrounded by a ring of 32 BChls and two rings of 16 carotenoids in the *Rba. sphaeroides* PufX-deficient RC-LH1 complex. In the similar *Tch. tepidum* used to prepare this Figure only one ring of carotenoids is present. Both types of RC-LH1 complex have five Trp residues per LH1 subunit at similar positions as inferred from protein sequence alignments. (c) Chemical structures of UVEM-1 (left) and UVEM-2 (right). Sources of the structures used in (a) and (b) and details of colour coding are described in Experimental Procedures.

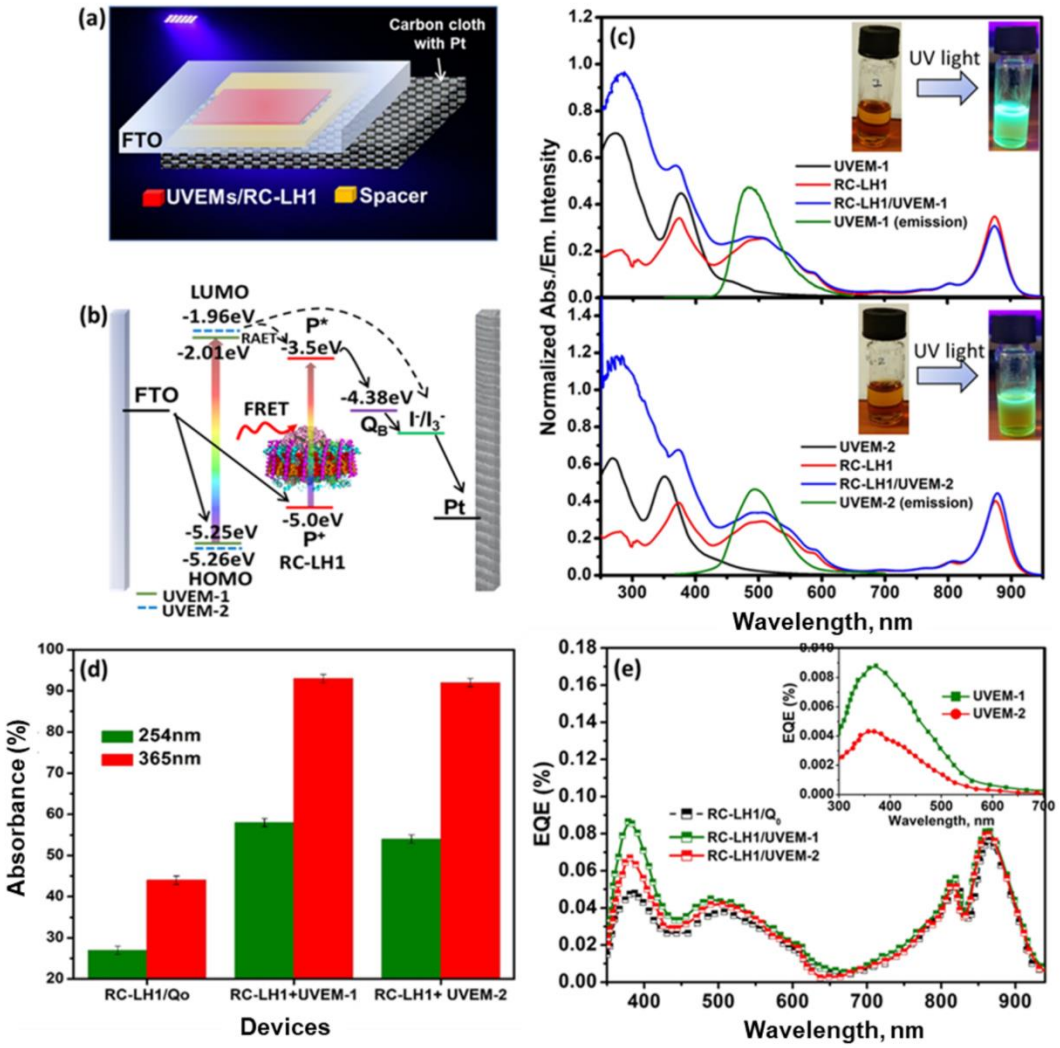

Figure 2. Device construction and components. (a) Schematic of BPEC architecture. (b) Energy level diagram of UVEM-only and RC-LH1/UVEM cells; energy transfer is to the RC-LH1 pigments (probably carotenoids), initiating P photoexcitation in the RC (FRET- Fluorescence resonance energy transfer and RAET- Radiation assisted energy transfer). (c) Optical spectra of RC-LH1, UVEMs and a 4:3 mixture of RC-LH1/UVEMs. (d) Percentage absorbance of UV light by RC-LH1 with ubiquinone-Q_0 or UVEMs. (e) EQE action spectra (inset shows spectra of UVEM-only control devices).

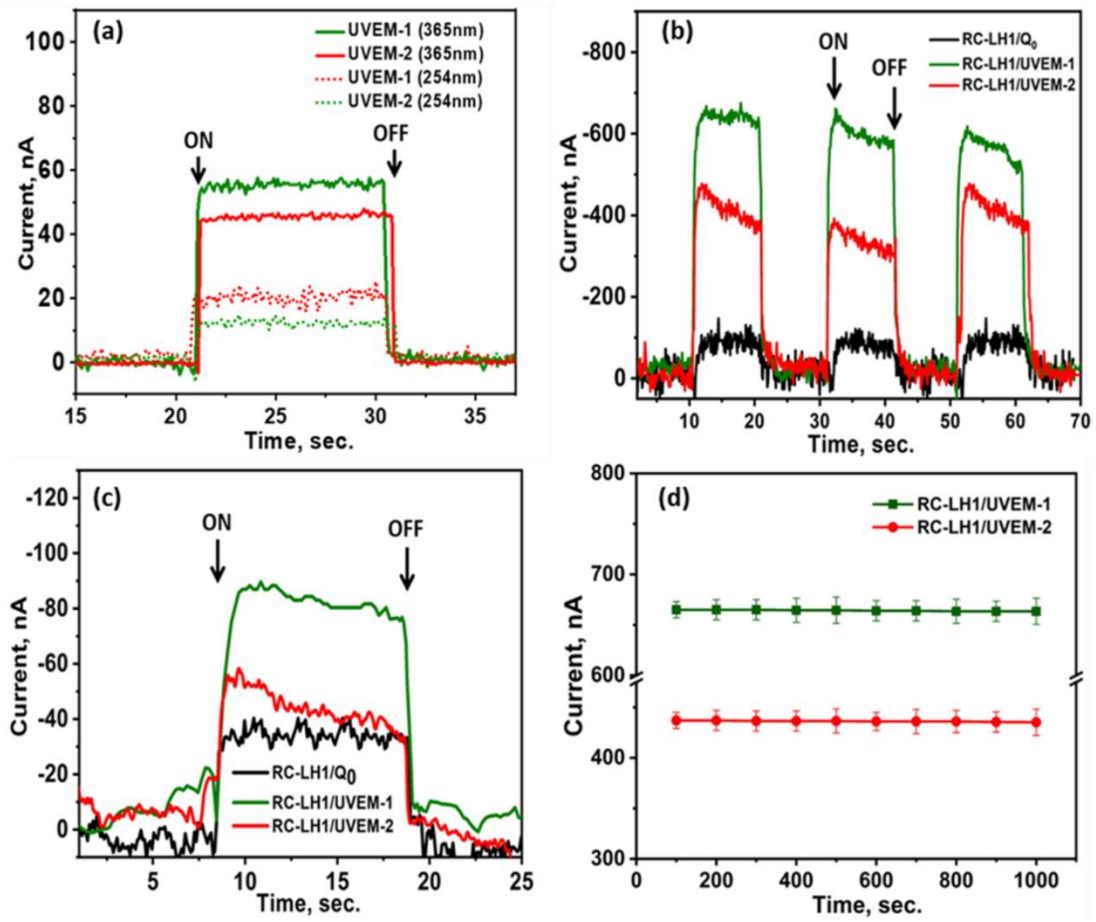

Figure 3. Cell photocurrents. (a) Photo-chronoamperometry of UVEM-only cells under 365 nm (left) and 254 nm (right) excitation. (b) Photo-chronoamperometry of RC-LH1 cells under 365 nm excitation. (c) Photo-chronoamperometry of RC-LH1 cells under 254 nm excitation. (d) Reproducibility of light-on/light-off photocurrent density at 100 s intervals with 365 nm excitation. For all panels 365 nm excitation was at 1350 μW cm^{-2} intensity and 254 nm excitation at 100 μW cm^{-2} intensity.

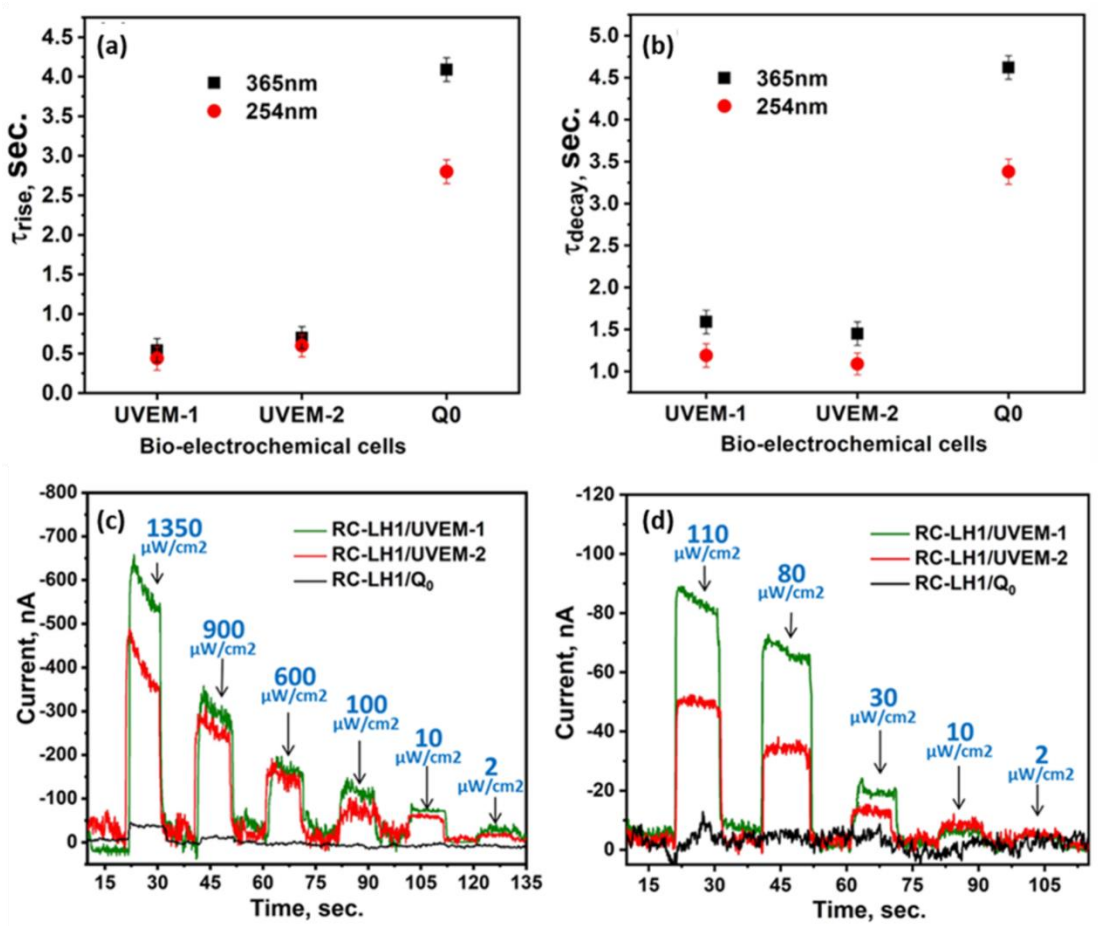

Figure 4. Speed and sensitivity of response to UV excitation. (a) Rise time (τ_{rise}) and (b) Decay time (τ_{decay}) of RC-LH1 BPECs with indicated electrolytes under UV illumination. These time constants are the time taken to achieve 90% of the maximum current or decay to 10% of the maximum current, respectively. (c) Photocurrent as a function of excitation intensity at 365 nm. (d) Photocurrent as a function of excitation intensity at 254 nm.

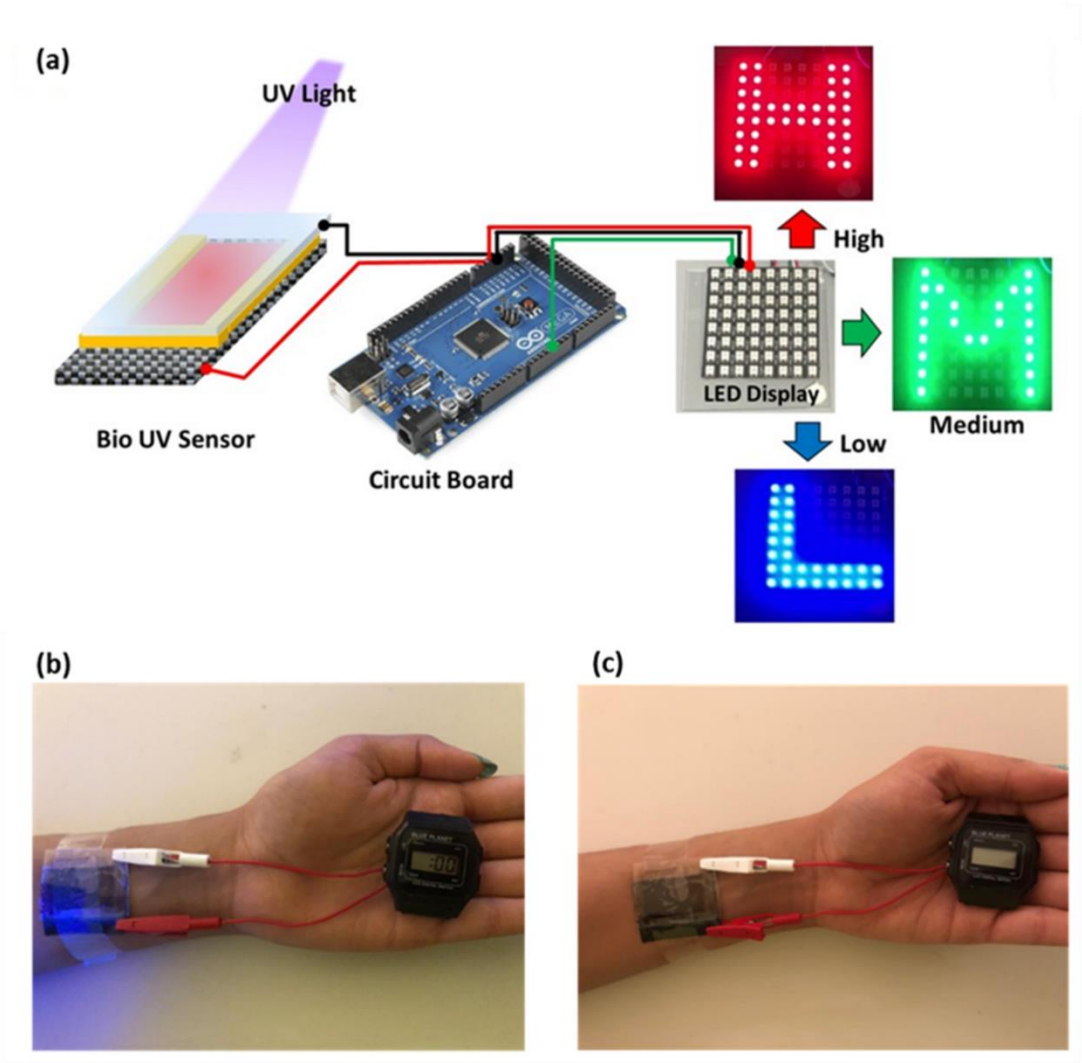

Figure 5. Schematic representation of possible device applications (RC-LH1+UVEMs). (a) Working model of a UV bio-sensor with a display powered by Arduino (Signs; H=High intensity light, M= medium intensity light and L=low intensity light). (b, c) Demonstration of a prototype wearable device powering a small display (b) when exposed to low UV intensity (200 µW cm^{-2}) (c) in the absence of UV in a dim room.

Table 1. Photocurrent response of BPECs under 365 nm or 254 nm excitation at maximum intensity.

Movie S1. Working prototype of BPEC UV-photodetector. Demonstration of UV detector being used to trigger an LED display board. The highest intensity of 365 nm UV light (1350-800 μW cm^{-2}) triggers a red “H”, medium intensity UV (800-100 μW cm^{-2}) triggers a green “M” and the lowest intensity of UV (100 to 2 μW cm^{-2}) triggers a blue “L”. The distance between bio-UV sensor and UV source for each category.

Device contents	**J_{sc} (nA/cm^2) at 254 nm**	**J_{sc} (nA/cm^2) at 365 nm**
RC-LH1/UVEM-1	86 (± 4)	665 (± 5)
RC-LH1/UVEM-2	49 (± 4)	437 (± 4)
RC-LH1/Q_0	37 (± 3)	120 (± 4)
UVEM-1	20 (± 3)	55 (± 2)
UVEM-2	12 (± 3)	45 (± 2)

Table 1. Photo-chronoamperometry of RC-LH1/UVEMs. Photocurrent response of BPECs under 365 nm or 254 nm excitation at maximum intensity.

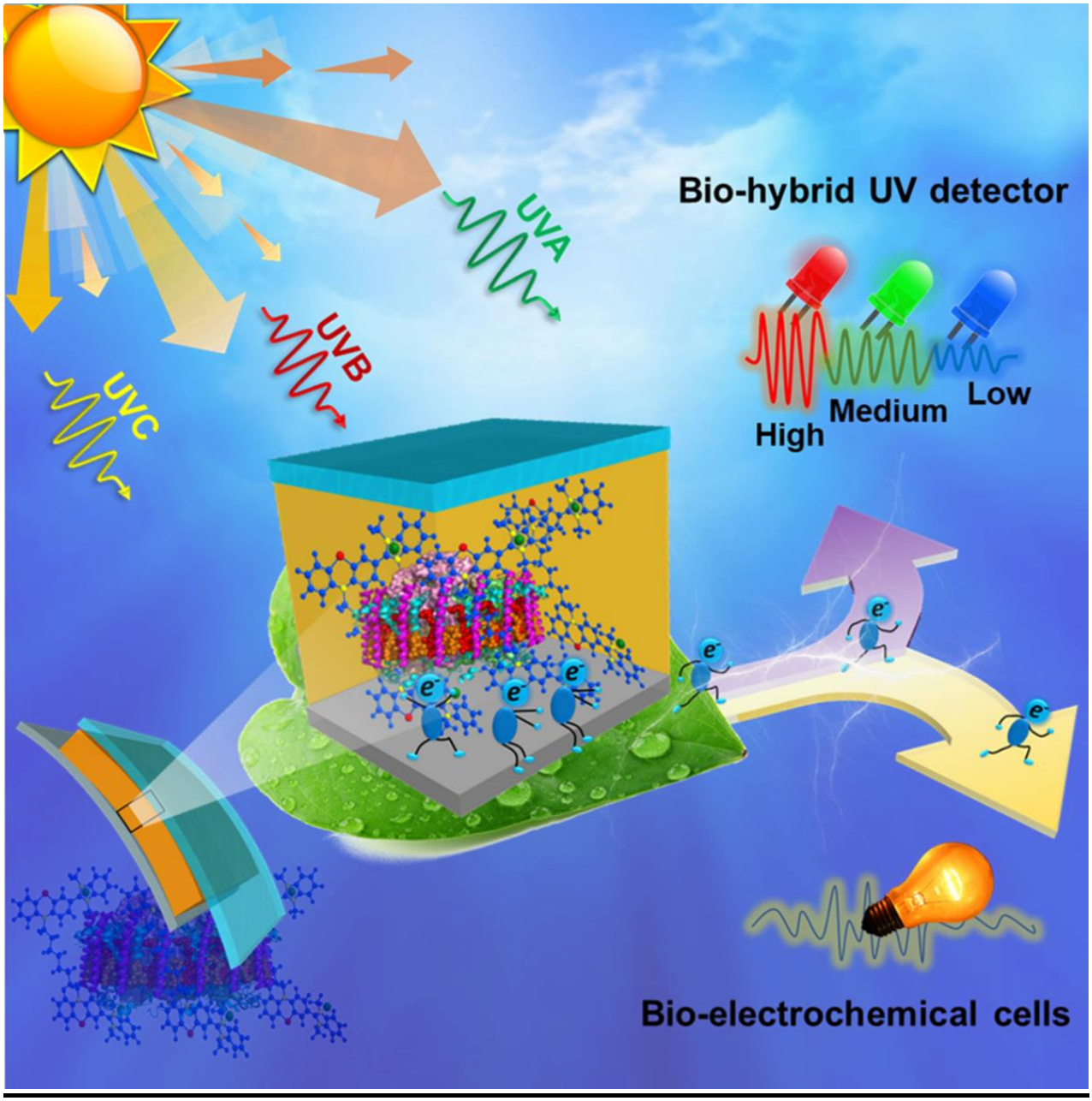
Bio-hybrid UV detector
UVA
UVB
UVC
High
Medium
Low
e⁻
Bio-electrochemical cells

Supplemental Information

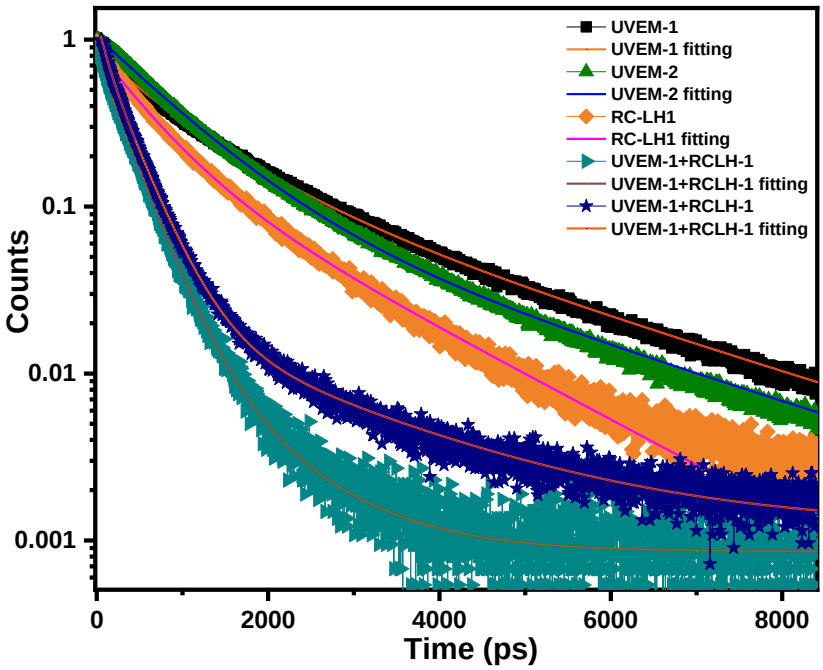

Figure S1. TRPL study. Related to Figure 2 b, c. Decay of phospholuminescence following excitation at 370 nm, with tri-exponential fits of the decay.

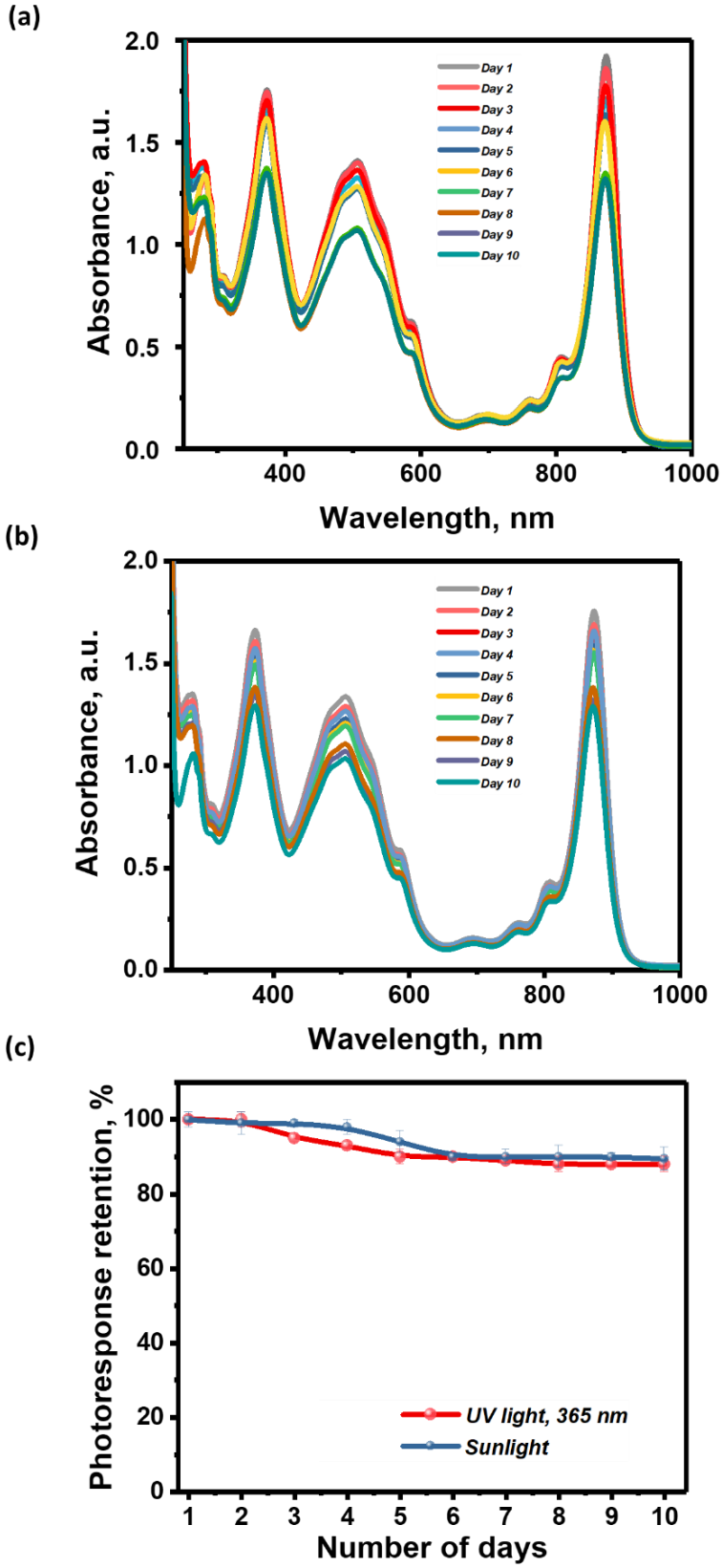

Figure S2. Stability of photosynthetic protein/UVEM mixture and device output. Related to figure 3 d. (a) Mixture exposed to 5-hour periods of sunlight for 10 days (b) Mixture exposed to 5-hour periods of high intensity UV for 10 days (c) Percentage of photocurrent response retained after sunlight or UV exposure.

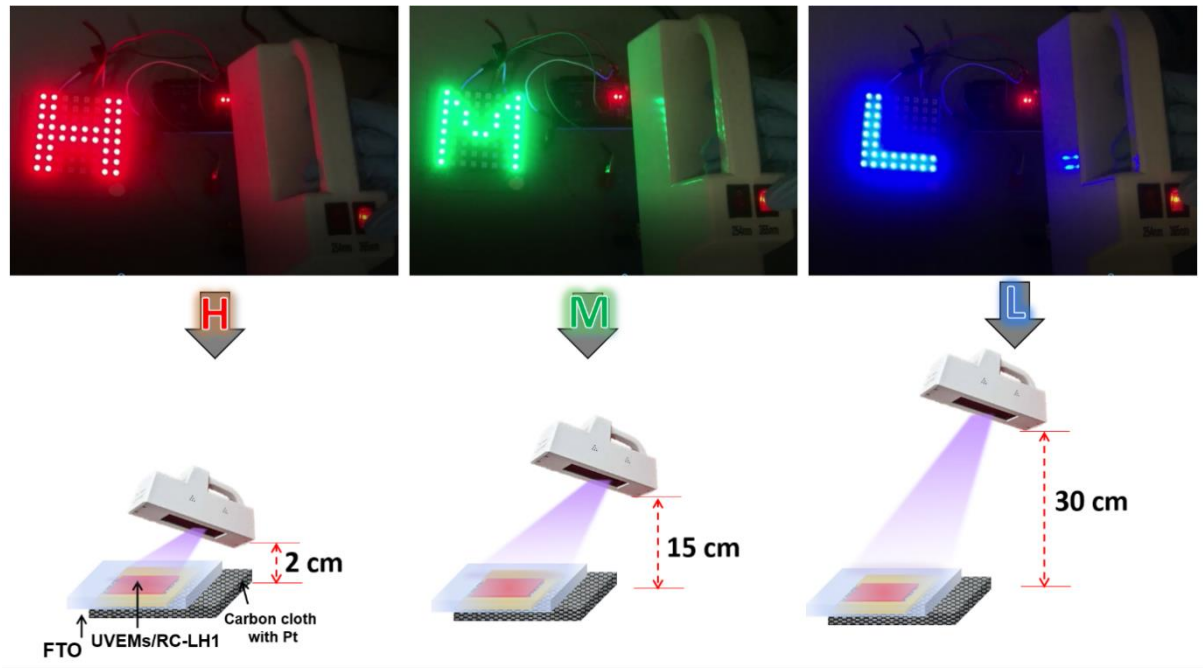

Scheme S1. Illustration of working BPEC UV-photodetector. Related to Movie S1 and Figure 5.

Sample	τ_1 (ps)	τ_2 (ps)	τ_3 (ps)	<τ> (ps)*	τ_{amp} (ps)#	χ^2	η_{FRET} (%)$
UVEM-1	202.5	923.96	2738	1728	1115	1.81	--
UVEM-2	821.5	821.56	2688	1415	1054	1.71	--
RC-LH1	48.84	543.01	1596	1064	725	1.64	--
UVEM-1/RC-LH1	71.57	326.11	469	335	289	0.80	74.1
UVEM-2/RC-LH1	96.8 0	330.74	749	539	404	0.91	61.6

Table S1. Time resolved PL measurement analysis of UVEM and RC-LH1 (phospholuminescence decay). Related to Figure 2 c. Parameters τ_1, τ_2 and τ_3 are excited state lifetimes, <τ> is the average lifetime, χ^2 is fitting parameter, η_{FRET} is energy transfer efficiency and τ_{amp} is the amplitude weighted lifetime.

*The average exciton lifetime, <τ> is calculated; $< \tau > = \sum A_i \tau_i^2 / \sum A_i \tau_i$

#The amplitude weighted lifetime, τ_{amp} is obtain using equation; $\tau_{amp} = \sum A_i \tau_i / \sum A_i$

$The percentage of energy transfer efficiency is calculated from the amplitude weighted donor lifetime, τ_{amp} in the presence and absence of the RC-LH1 molecules using following equation.

$$\eta_{FRET} = \left(1 - {}^{\tau_{RC-LH1+UVEM}}/_{\tau_{UVEM}}\right) \times 100$$

UV intensity, μW/cm^2	UVEM-1		UVEM-2	
(365 nm)	τ_{rise} (sec.)	τ_{decay} (sec.)	τ_{rise} (sec.)	τ_{decay} (sec.)
1350	0.54 (± 0.05)	1.60 (± 0.06)	0.70 (± 0.06)	1.69 (± 0.05)
900	0.60 (± 0.06)	1.82 (± 0.09)	0.72 (± 0.07)	1.83 (± 0.10)
600	1.28 (± 0.08)	2.12 (± 0.10)	1.64(± 0.10)	2.26 (± 0.11)
100	2.33 (± 0.09)	2.47 (± 0.13)	2.43 (± 0.12)	2.61 (± 0.13)
10	2.84 (± 0.10)	2.41 (± 0.18)	2.92 (± 0.15)	2.50 (± 0.15)
2	3.95 (± 0.13)	4.16 (± 0.20)	4.02 (± 0.16)	4.56 (± 0.20)
UV intensity, μW/cm^2	UVEM-1		UVEM-2	
(254 nm)	τ_{rise} (sec.)	τ_{decay} (sec.)	τ_{rise} (sec.)	τ_{decay} (sec.)
110	0.44 (± 0.06)	1.29 (± 0.07)	0.60 (± 0.08)	1.40 (± 0.08)
80	0.69 (± 0.08)	1.61 (± 0.07)	0.99 (± 0.09)	1.68 (± 0.10)
30	2.48 (± 0.11)	2.41 (± 0.10)	2.66 (± 0.10)	2.47 (± 0.11)
10	2.67 (± 0.10)	2.81 (± 0.12)	2.82 (± 0.12)	2.88 (± 0.11)
2	3.06 (± 0.14)	2.98 (± 0.14)	3.21 (± 0.15)	3.31 (± 0.113)

Table S2. Device responsiveness and sensitivity. Related to Figure 4. Consolidated rise time, decay time and sensing range observed for RC-LH1/UVEMs based photodetector.